Int. J. Solids Structures Vol. 23, No. 10, pp. 1341–1356, 1987
Printed in Great Britain.

0020–7683/87 $3.00+ .00

DEFLECTION AND SNAPPING OF SPHERICAL CAPS

G. W. BRODLAND and H. COHEN
Department of Civil Engineering, University of Manitoba, Winnipeg, Manitoba, Canada R3T 2N2

(*Received* 1 *August* 1986; *in revised form* 22 *January* 1987)

Abstract—This paper treats the finite axisymmetric deflection and snapping of spherical caps which are point loaded at the apex and simply supported at the boundary. The problem is formulated using a stationary potential energy principle and solved numerically. The response of caps up to critical loads and into the postbuckling regime to eversion and beyond is studied and detailed. Phenomena such as snapthrough, snapback, multiple load free equilibria, eversion and irreversibility, are found to occur.

1. INTRODUCTION

The development of non-linear continuum mechanics seemed to reach a pinnacle of activity some 25 years ago. No doubt, this was spurred on by success during the previous decades in solving problems arising in non-linear elasticity and non-linear fluid mechanics. The advent of new non-linear materials, not adequately described by these earlier solutions, contributed to the activity.

It was only natural that shell theory would be affected by the same enthusiasm towards constructing non-linear theories. The outcome of this activity has in large measure been successful, especially in laying a firm foundation for the non-linear theory. Two comprehensive treatments detailing research of the recent period, differing somewhat in viewpoint, can be found in the articles of Naghdi[1] and of Libai and Simmonds[2].

Perhaps one of the disappointments of the research on the non-linear shell theories is that there are not more analytical solutions to the governing equations. Unquestionably, this stems from the immense complexity of the theory. We cite Antman[3], as a researcher who has addressed some of the issues.

The overall situation is in reality better than it appears at first sight. The availability of high-speed computers and the development of new numerical techniques have given rise to the numerical treatment of important technological problems. Additionally, the overall literature on shells is so vast, e.g. see the bibliographies of Nash[4, 5], that for most problems one can find a reasonable body of knowledge to use as a starting point.

New technologies require solutions to problems largely of academic interest 25 years ago. The advent of rubber caps as an integral part of the spring–actuator mechanism in computer and typewriter keyboards, push button telephones and a host of other similar applications has generated a need for large deformation solutions of rubber-like axisymmetrical shells.

The problem we address in this paper is to deal with the large axisymmetric deformation of spherical rubber caps loaded at their apex by a point load and simply supported at their boundary. We consider the full range of geometries from very shallow to full hemispherical caps. We are interested in *buckling or snapping phenomena, post-buckling behaviour to complete eversion, and return from the everted to the virgin state.* Our method of attack is numerical; our aim is insight. Thus, the value of our study may be two-fold. First, to contribute to the the design and engineering of actuator caps or related technological devices, and second, to provide the genus for ideas on extracting analytical solutions from the non-linear theories.

As indicated above, there is a literature on the problem of interest herein. To begin with, Kaplan[6] in 1974 gave a review of the situation regarding the deformation and buckling of complete spherical shells and spherical caps. Most of this work is concerned with pressure loading and clamped edge conditions. The former condition gives rise to

follower load interference and stability effects not at issue for our problem; the latter condition unfortunately prevents the full range of phenomena encountered for the freely-supported shell. Much of the behaviour identified herein is *unique* to *incomplete* spherical shells with *simply supported edges* and *apical point loads*. The behaviour of clamped, complete, or pressure loaded spheres are very different, and are discussed in Refs [7–10], and their respective bibliographies.

We summarize briefly those studies related to this research. The first non-linear analysis was published by Biezeno in 1935[11]. In 1957, Chien and Hu[12] considered the more general problem of a spherical cap subject to an axisymmetric ring load, which in the limiting case of apex loading, produced results similar to Biezeno. Ashwell[13] in 1959 carried out a clever analysis, based on *Love's principle of applicable surfaces*, in which he used linear shallow shell theory to fit together inner everted and outer undeformed spherical regions of the shell. The first numerical analysis of the point loaded cap was done by Archer in 1962[14]. In the same year, Evan-Iwanowski *et al.* and subsequently in 1964, Loo and Evan-Iwanowski published extensive experimental results for point loaded caps[15, 16]. Also in 1964, Wilson and Spier[17] considered the deep spherical shell using a finite-difference technique, but restricted the analysis to loads less than critical. Mescall[18, 19] in the mid-1960s, presented the first numerical analysis of load–deflection behaviour into the post-buckling region. Further numerical studies were carried out by Bushnell[20] in 1967 and more recently by Parisch[21] in 1979. The latter gave the shape of the meridian contours for shells deformed to eversion.

We now summarize the content of this paper. In Section 2, we give the basic geometrical and physical equations that govern the finite strain and rotation analysis of spherical shells. These include a statement of the governing variational principle and an expression for the shell surface strain energy function. The latter is derived for a shell, which in its undeformed configuration, is a homogeneous isotropic sphere of uniform thickness, and the three-dimensional material properties of which are characterized as *Mooney–Rivlin hyperelastic*.

As already mentioned, our approach is to solve the problem at hand through a numerical scheme. This is developed in Section 3 for shell deformations free of any restriction on strain or rotation. The contour of the deformed shell meridian is first represented by a discrete number of segmental functions whose nodal positions and slopes comprise new unknown variables in the problem. These are then determined so as to correspond to stationary values of the total potential energy of the shell and hence, according to our variational principle, correspond to a deformed equilibrium configuration. Stationary points are found by a technique which utilizes the gradient and Hessian of the potential energy surface and which is accelerated using line search.

In Section 4, we present detailed results. These are comprised of *load–deflection curves*, *critical loads*, and *deformed contours* for shells which vary from very shallow to very deep. The results are compared with those available in the cited literature. For sufficiently thin shells, we find a full range of deformation behaviour involving *snapthrough*, *snapback*, *eversion* and *irreversibility* from eversion back to the virgin state. Thicker shells exhibit a somewhat more restricted range of behaviour. Finally, we discuss the confirmation of these predictions by our own experimentation with spherical rubber caps.

2. THE BASIC EQUATIONS

The equations of non-linear shell theory consist of a system of differential and algebraic equations. These are comprised of the equilibrium equations, the strain–displacement equations, and the constitutive relations. The theory governs large deformations which are comprised generally of finite strain and rotation. For the axisymmetric deformation of shells of revolution, a sample of these equations is provided in the paper of Cohen and Pastrone[22]. The sphere problem of interest here is usually treated on the basis of a suitably simplified set of governing differential equations. Such is certainly the case for the literature cited in the Introduction. An alternative to solving such a system is to employ a *variational principle*. This is the line of attack that we shall develop in this paper.

Since the analysis herein is confined to axisymmetric deformations, we begin by reviewing some of the geometry associated with the axisymmetric deformation of shells of revolution. The deformed configuration is assumed in the form

$$\mathbf{x} = \mathbf{r} + n(s)\mathbf{n}, \qquad \mathbf{r} = r(s)\mathbf{e}_r(\phi) + z(s)\mathbf{e}_z \tag{1}$$

where $\mathbf{r}$ is the position vector to a point on the deformed reference surface σ. In writing eqn $(1)_2$, we have employed a cylindrical polar coordinate system (r, ϕ, z) with an associated orthonormal basis of vectors $(\mathbf{e}_r, \mathbf{e}_\phi, \mathbf{e}_z)$ and with $\mathbf{e}_z$ along the axis of symmetry. The parameters (s, ϕ) are surface coordinates which measure arc length along a meridian and angle along a parallel circle, respectively. These curves comprise lines of curvature on σ. The unit outward normal $\mathbf{n}$ to σ is given by

$$\mathbf{n} = \cos\theta\mathbf{e}_z + \sin\theta\mathbf{e}_r \tag{2}$$

in terms of the angle θ between the normal and the axis of symmetry. In eqns (1), n measures distances along $\mathbf{n}$ to a generic point $\mathbf{x}$ in the shell.

The undeformed configuration of the shell is given by eqns (1) with the quantities $\mathbf{x}$, $\mathbf{r}$, $\mathbf{n}$, r, ϕ, z, n, θ, s, replaced by $\mathbf{X}$, $\mathbf{R}$, $\mathbf{N}$, R, Φ, Z, N, Θ, S, respectively. For the problem at hand, where the undeformed shell is spherical, the pertinent functions are

$$R = a\sin(S/a), \qquad Z = a\cos(S/a), \qquad \Phi = S/a \tag{3}$$

where a is the radius of the shell mid-surface $\mathscr{S}$ and S is the arc length along a meridian measured from the pole. We assume also that the thickness h of the shell is constant. The requirement that the reference surface $\mathscr{S}$ be the undeformed mid-surface imposes the condition $-h/2 \leqslant N \leqslant h/2$.

In order to completely characterize the deformation of the shell, we assume that $\mathscr{S}$ map into σ, and further that the deformation satisfy *a relaxed Kirchhoff hypothesis*. The latter condition means that the deformation carries the direction of $\mathbf{N}$ into the direction of $\mathbf{n}$, and so transverse shear deformation is being ignored. However, unlike the classical Kirchhoff hypothesis, there is no constraint upon the stretch along the normal. In particular, this means that generally σ will not be the mid-surface of the deformed shell. To make the deformation mathematically explicit, we need to prescribe the functions

$$s = s(S), \qquad \phi = \Phi, \qquad n = n(N). \tag{4}$$

Straightforward computations employing eqns (1)–(4) lead to the standard results

$$v_1 = \frac{(1+k_1 n)}{(1+K_1 N)}\lambda_1, \qquad v_2 = \frac{(1+k_2 n)}{(1+K_2 N)}\lambda_2, \qquad v_3 = \frac{\mathrm{d}n}{\mathrm{d}N} \tag{5}$$

for the principal stretches v_i, $i = 1, 2, 3$, at an arbitrary point of the shell. The quantities λ_α, $\alpha = 1, 2$, are the principal stretches on σ given by

$$\lambda_1 = \frac{\mathrm{d}s}{\mathrm{d}S}, \qquad \lambda_2 = \frac{r}{R}. \tag{6}$$

The principal stretches are along the lines of curvature of σ, the principal curvatures of which k_α, $\alpha = 1, 2$, are given by

$$k_1 = \frac{\mathrm{d}\theta}{\mathrm{d}s}, \qquad k_2 = \frac{\sin\theta}{r}. \tag{7}$$

We note that $K_1 = K_2 = 1/a$ in eqns (5).

Other quantities associated with the deformation can be calculated. In particular, the ratio of corresponding volume elements $(g/G)^{1/2}$ arising from the deformation is given by

$$(g/G)^{1/2} = \frac{(1+(k_1+k_2)n+k_1k_2n^2)}{(1+(K_1+K_2)N+K_1K_2N^2)} v_3(a/A)^{1/2} \tag{8}$$

where $(a/A)^{1/2}$ is the ratio of corresponding reference surface elements specified by

$$(a/A)^{1/2} = \lambda_1\lambda_2. \tag{9}$$

In this work, we shall confine attention to shells constructed of rubber-like materials. These are generally *incompressible* and we impose this as a constraint on the deformation, namely, we assume

$$(g/G)^{1/2} = 1. \tag{10}$$

To extract the implication of eqn (10), we combine eqns $(5)_3$, (8), (9) and (10) to obtain a differential relation in dn/dN. We integrate this relation and invoke approximations common in thin shell theory to arrive at an explicit form for eqn $(4)_3$, namely

$$n = (N/\lambda_1\lambda_2)+[(\lambda_1\lambda_2/a)-(k_1+k_2)/2](N/\lambda_1\lambda_2)^2 - \{(k_1+k_2)[(\lambda_1\lambda_2/a)-(k_1+k_2)/2]+k_1k_2/3\}(N/\lambda_1\lambda_2)^3. \tag{11}$$

In the preceding discussion, we have summarized the required geometrical background for our study. In order to deal with the mechanics of the shell, we must ascribe its material properties. This we do by assuming the shell material to be *hyperelastic*. In other words, there exists for the material a strain energy density function ε, measuring the energy stored by the deformation per unit volume of the shell. We assume ε to be of the Mooney–Rivlin form; thus the material is homogeneous, isotropic and incompressible, with ε given by

$$\varepsilon = c_1(I_1-3)+c_2(I_2-3) \tag{12}$$

where c_1, c_2 are material constants

$$I_1 = v_1^2+v_2^2+v_3^2, \qquad I_2 = v_1^2v_2^2+v_1^2v_3^2+v_2^2v_3^2 \tag{13}$$

and

$$v_3 = 1/v_1v_2. \tag{14}$$

We remark that for small strains, eqns (13) model the linear behaviour of incompressible materials when the material constants are set to $c_1 = 5G/8$ and $c_2 = -G/8$, where G is the material shear modulus. Other reasonable choices for c_1 and c_2 exist; however, *this* choice provides the best simulation of linear behaviour as strains become larger. This will permit calculations in Section 4 which can be compared with the results published in the literature.

The objective of shell theory is to develop a two-dimensional theory of thin three-dimensional bodies. In other words, we need a constitutive relation of the type

$$\sigma = \sigma(\lambda_\alpha, k_\alpha) \tag{15}$$

for a strain energy σ per unit area of the undeformed reference surface $\mathscr{S}$. Equation (15) has the functional form appropriate to represent a homogeneous isotropic shell.

In order to obtain an explicit form for eqn (15), we compute the total strain energy $\mathscr{E}$ in the shell in terms of σ and ε, respectively. The result is

$$\mathscr{E} = \int_{\mathscr{S}} \sigma A^{1/2} = \int_{\mathscr{V}} \varepsilon G^{1/2} \tag{16}$$

where $\mathscr{V}$ denotes the undeformed shell volume and for convenience, we have dropped explicit dependence on the Euclidean surface and volume differentials. From eqn $(16)_2$, by arguments now standard in continuum mechanics, we conclude immediately that

$$\sigma = \int_{-h/2}^{h/2} \varepsilon\{v_\alpha(N)\}\,(1+N/a)^2\,\mathrm{d}N \tag{17}$$

where eqn (14) has been used to eliminate v_3. To evaluate eqn (17), we substitute eqn (11) into eqns $(5)_{1,2}$. The result can then be used in eqns (13) and (14) to yield I_1 and I_2 in terms of N and the surface quantities λ_α, k_α. Finally, elimination of I_1 and I_2 from eqn (12) and substitution of the result into eqn (17) yields an integrand which can be dealt with. We obtain a suitable constitutive relation after dropping terms negligible within the framework of thin-shell theory. The result is

$$\begin{aligned}\sigma = {} & c_1[\{\lambda_1^2+\lambda_2^2+\lambda_1^{-2}\lambda_2^{-2}-3\}h \\ & +\{a_1^2(1+3\lambda_1^{-4}\lambda_2^{-2})+a_2^2(1+3\lambda_1^{-2}\lambda_2^{-4})+4a_1a_2\lambda_1^{-3}\lambda_2^{-3}\}h^3/12] \\ & +c_2[\{(\lambda_1^2-a_1^2h^2/4)^{-1}+(\lambda_2^2-a_2^2h^2/4)^{-1}+\lambda_1^2\lambda_2^2-3\}h \\ & +\{a_1^2\lambda_2^2+4a_1a_2\lambda_1\lambda_2+a_2^2\lambda_1^2\}h^3/12]\end{aligned} \tag{18}$$

where

$$a_1 = (k_1/\lambda_2)-(\lambda_1/a), \qquad a_2 = (k_2/\lambda_1)-(\lambda_2/a). \tag{19}$$

Since transverse shear deformation is ignored in the basic formulation, the preceding constitutive relation, eqn (18), contains no energy terms associated with transverse shear. For details of the calculation we refer the reader to Brodland[23]; for the analytic procedure leading to eqn (18) we acknowledge the work of Libai and Simmonds[24], who utilized a similar line of attack in dealing with cylindrical shells. Similar shell theories have recently been proposed by Simmonds[25] and Taber[26].

The final ingredient of the theoretical basis for our analysis lies in the variational principle alluded to in the opening paragraph of this section. We define the *total potential energy*, $\mathscr{W}$, of the shell to be the functional of the deformed configuration given by

$$\mathscr{W} = \mathscr{E} - Pw \tag{20}$$

where P is the magnitude of the vertical load at the shell apex and w is the axial deflection at the load. We now lay down the requirement that *deformed equilibrium configurations of the spherical shell are those which correspond to local stationary values of* $\mathscr{W}$. The preceding is the governing variational principle.

3. THE NUMERICAL ANALYSIS

The basis of the numerical analysis lies in approximating the meridian configurations by a finite number of smooth segments of a prescribed shape. These segments are separated by adjacent boundary points $N_j, j = 1, 2, \ldots, m+1$, called *nodes*. The shape of each of the m segments comprising the meridian is represented by an explicit two-parameter family of *segmental functions* S_j. These start and end at the neighbouring nodal points N_j and N_{j+1}, respectively. The slope of adjacent segmental functions S_j, S_{j+1}, is required to be continuous at their common node N_{j+1}. The location of each node N_j is specified by its coordinates

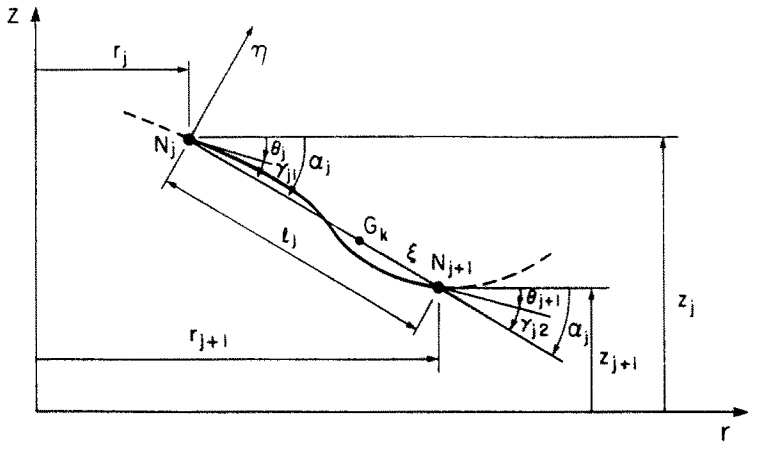

Fig. 1. Segment formulation.

(r_j, z_j). The parameters γ_{j1}, γ_{j2}, which will appear in the jth segmental function, are determined by specifying θ_j at N_j and by using the continuity at N_{j+1}. In summary, we remark that the approximate representation of the meridian will be controlled by specifying $n = 3(m+1)$ variables (r_j, z_j, θ_j), which for convenience we denote by x_i, $i = 1, 2, \ldots, n$.

The segmental functions S_j are defined with respect to a conveniently chosen local rectangular Cartesian coordinate system (ξ, η), whose origin is at N_j and whose ξ-axis passes through N_{j+1}. The coordinate ξ is non-dimensional and normalized so that the interval of definition of S_j is $0 \leqslant \xi \leqslant 1$. The coordinate η has the dimension of length. For a graphic representation of the situation, we refer the reader to Fig. 1.

We assume S_j to be given explicitly by the formula

$$\eta_j(\xi) = \{\gamma_{j1}\xi(1-2\xi+\xi^2)+\gamma_{j2}\xi(-\xi+\xi^2)\}l_j \tag{21}$$

where l_j is the distance between the boundary nodes N_j, N_{j+1}, namely

$$l_j = \{(r_{j+1}-r_j)^2+(z_{j+1}-z_j)^2\}^{1/2} \tag{22}$$

and $\gamma_{j\alpha}$, $\alpha = 1, 2$, the parameters referred to above, are required to be small relative to unity, i.e. $\gamma_{j\alpha} \ll 1$. This condition does not restrict *global* strains or rotations, but rather restricts the maximum spacing of nodes so that displacements and slopes with respect to the *local* (ξ, η) coordinate system are small. The orientation of the local (ξ, η) coordinate system relative to the global axes (r, z) is defined by the angle α_j between the ξ- and r-axes. It is given by

$$\alpha_j = \tan^{-1}\{(z_j-z_{j+1})/(r_{j+1}-r_j)\}. \tag{23}$$

If we now differentiate eqn (21) with respect to ξ, then from the smallness of $\gamma_{j\alpha}$, we see immediately that $(\mathrm{d}\eta/l_j\,\mathrm{d}\xi)$ represents the angle between the tangent line to S_j and the ξ-axis. Indeed, we also see that γ_{j1} and γ_{j2} are just the angles made by S_j with the ξ-axis at the nodes N_j and N_{j+1}, respectively. Furthermore, it is obvious that $(\mathrm{d}^2\xi/l_j^2\,\mathrm{d}\eta^2)$ defines the principal curvature of S_j to the same order of approximation.

The position and slope of the segmental meridian contour S_j are given in terms of the global (r, z) coordinate system by the equations

$$r(\xi) = r_j(1-\xi)+r_{j+1}\xi+\eta(\xi)\sin\alpha_j \tag{24}$$

$$z(\xi) = z_j(1-\xi)+z_{j+1}\xi+\eta(\xi)\cos\alpha_j \tag{25}$$

$$\theta(\xi) = \left\{\alpha_j - \frac{1}{l_j}\frac{\mathrm{d}\eta}{\mathrm{d}\xi}(\xi)\right\}. \tag{26}$$

The principal stretches and principal curvatures of the shell reference surface, eqns (6) and (7), respectively, are for the jth segment given respectively by

$$\lambda_1 = \frac{l_j}{L_j}, \qquad \lambda_2 = \frac{r(\xi)}{R(\xi)} \tag{27}$$

and

$$k_1 = \frac{-1}{l_j^2}\frac{d^2\eta}{d\xi^2}(\xi), \qquad k_2 = \frac{\sin\theta(\xi)}{r(\xi)}. \tag{28}$$

The above formulation is valid for *arbitrarily large* strains and rotations.

The principle enunciated at the end of Section 2 provides the *modus operandi* for completing the numerical analysis and finding the equilibrium configurations of the shell. To begin with, the integral involved in eqn $(16)_1$ to calculate the total strain energy is one dimensional, namely

$$\mathscr{E} = 2\pi \int_0^S R\sigma \, dS. \tag{29}$$

To evaluate eqn (29), first we write the surface strain energy σ_j, for the segment S_j, in terms of the variables x_i by substitution of eqns (21)–(28) into eqn (18). Next, we use *Gauss quadrature* to numerically integrate eqn (29) over the segment S_j, and obtain the total strain energy as the sum

$$\mathscr{E} = 2\pi \sum_{j=1}^{m} \sum_{k=1}^{p} R(G_k) f_k \sigma(G_k). \tag{30}$$

In eqn (30), the G_k, $k = 1, 2, \ldots, p$, are Gauss points on the ξ-interval $[0, 1]$, and the f_k are the associated weighting factors. If we substitute eqn (30) into eqn (20), then the total potential energy is now of the form

$$\mathscr{W} = \mathscr{W}(x_i). \tag{31}$$

By virtue of eqn (31), the variational principle now assumes the form of an n-variable stationary value problem. The boundary conditions at the free edge of the shell now enter the problem as constraints on the variables x_i. We observe that our problem has been reduced to a standard *non-linear programming problem.*

The most efficient techniques for solving the non-linear programming problem take the form of *descent methods* which utilize first and possibly higher order derivatives of the hypersurface $\mathscr{W}(x_i)$ with respect to the variables x_i. The method employed here make use of a Taylor's expansion of $\mathscr{W}(x_i)$ to second-order terms in the change d_i of x_i, i.e. we write

$$\mathscr{W}(\mathbf{x}+\mathbf{d}) = \mathscr{W}(\mathbf{x}) + \mathbf{g}\cdot\mathbf{d} + \tfrac{1}{2}\mathbf{d}^T\cdot\mathbf{H}\mathbf{d} \tag{32}$$

where for convenience we have employed an obvious vector notation and have set

$$\mathbf{g} = \operatorname{grad}\mathscr{W}, \qquad \mathbf{H} = \operatorname{grad}^2\mathscr{W}. \tag{33}$$

We note that $\mathbf{g}$ is a vector called the *gradient* of $\mathscr{W}$ and $\mathbf{H}$ is a linear operator called the *Hessian* of $\mathscr{W}$.

Equation (32) provides a parabolic approximation to the potential energy hypersurface at point $\mathbf{x}$. To minimize the value of the former, we choose

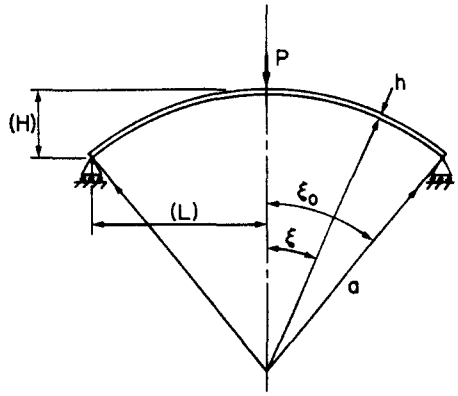

Fig. 2. Freely supported spherical cap.

$$\mathbf{d} = -\mathbf{H}^{-1}\mathbf{g}^T. \tag{34}$$

The value of $\mathbf{d}$ provided by eqn (34) can be used to iterate $\mathbf{x}$ towards the critical value $\mathbf{x}_{stat}$ of $\mathscr{W}$. Indeed, repeated iteration using eqns (33) and (34) provides a sequence of values $\mathbf{x}_r$ converging to $\mathbf{x}_{stat}$.

In order to accelerate the numerical convergence, we employ a *line search technique*. This entails obtaining $\mathbf{x}_{r+1}$ from the formula

$$\mathbf{x}_{r+1} = \mathbf{x}_r + \alpha \mathbf{d}_r \tag{35}$$

where α is determined by trial and error to be the value for which $\mathscr{W}$ is an *extreme* along the line defined by $(\mathbf{x}_r, \mathbf{d}_r)$. This process is numerically efficient by virtue of the fact that multiple evaluations of $\mathscr{W}$ require considerably less computing time than calculation of $\mathbf{d}_r$.

4. RESULTS AND DISCUSSION

The axisymmetric deformation of the point loaded spherical shell shown in Fig. 2 is characterized by two non-dimensional geometric parameters. The first of these is the shell half angle ξ_0. The other is a parameter λ defined by

$$\begin{aligned} \lambda^2 &= [12(1-\nu^2)]^{1/2}(a/h)\sin^2\xi_0 \\ &\cong [12(1-\nu^2)]^{1/2}(2H/h). \end{aligned} \tag{36}$$

The approximate form of eqns (36) is valid for sufficiently small ξ_0. The parameter ξ_0 provides a measure of the *depth* of the shell. The shell may be characterized as *shallow* when eqn $(36)_2$ holds, i.e. if $\xi_0 \cong 2H/L$. The parameter λ^2 essentially is a measure of *shell thickness*. Large λ^2 values are associated with *thin* shells.

The literature cited in the introductory section as pertinent to the problem at hand restricts consideration to linear elastic response which is characterized by the usual elastic moduli E and ν. As already mentioned, we can choose the Mooney–Rivlin constants c_1, c_2 to model linear incompressible materials with arbitrary Young's modulus E and Poisson's ratio $\nu = 0.5$[23]. It is then convenient to nondimensionalize the load P and apex deflection w by defining new variables P^* and w^* according to

$$P^* = Pa/Eh^3, \qquad w^* = w/H. \tag{37}$$

Our aim is to study the axisymmetric behaviour of spherical caps over as wide a range of geometries and loads as possible. The experimental research of Evan-Iwanowski *et al.*[15] and the numerical research of Bushnell[20] shows that caps with $\lambda^2 > 100$ can exhibit asymmetric deformations. Hence, attention is restricted to caps with $\lambda^2 \leqslant 100$.

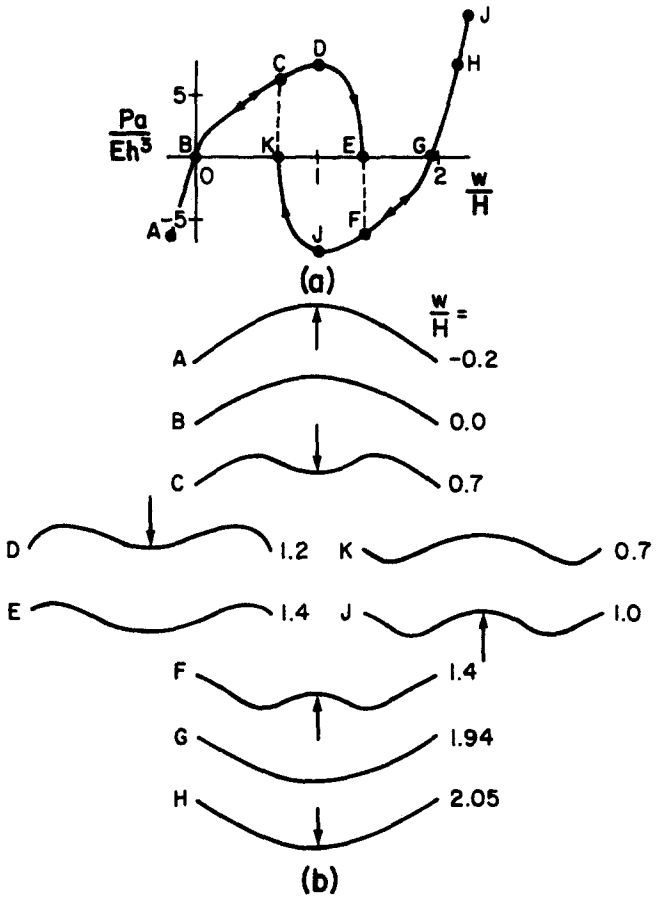

Fig. 3. Load–deflection curve and meridian contours for $\xi_0 = 22.5°$ and $\lambda^2 = 100$.

The full range of cap geometries is studied by considering shells of half angle 5°, 22.5° and 90°; λ^2 values of 16, 36, 64 and 100 are used to show the effects of thickness variation. The numerical procedure requires 8 elements to model shallow caps ($\xi_0 = 5°, 22.5°$) and 16 elements to model hemispheres ($\xi_0 = 90°$).

The numerical analysis was carried out by specifying apex *displacement* rather than *load*. This allowed both stable and unstable equilibrium states to be observed and the mechanism of snapping to be clearly demonstrated. Figure 3 shows the load–deflection curves and meridian contours for a cap with $\xi_0 = 22.5°$ and $\lambda^2 = 100$. The correspondence between meridian contours and points on the load–deflection curve is indicated by upper case letters. The initial state is B. State A is a cap with outward load and deflection. Increasing inward deflection produces increasing load up to a critical point D followed by a decrease in load to zero at E. States from D to E are unstable as the load carrying capacity of the shell decreases with increasing displacement. These states can, however, be demonstrated experimentally by specifying displacement rather than load.

If *load* rather than *displacement* is specified, loading proceeds along the path A–B–C–D as before, but a slight increase above the load carried at D produces a snapping to point H. The load at D is called the *critical load* P_c; the transition from configuration D across to configuration H is called *snapthrough*. Note that snapthrough involves a significant change in apex displacement for an infinitesimal change in load. Further loading occurs along H to J where large strains occur. Reverse load-governed deflection occurs along path J–H–G–F–J. New meridian configurations are produced along H–G–F–J. From J, snapthrough occurs to state A.

If *displacement* is controlled rather than *load*, loading occurs along A–B–C–D–E, and the shell then snaps from E to a new configuration F. This behaviour is known as *snapback*. Rather than having a large dimple at E, it has snapped to a new shape involving complete

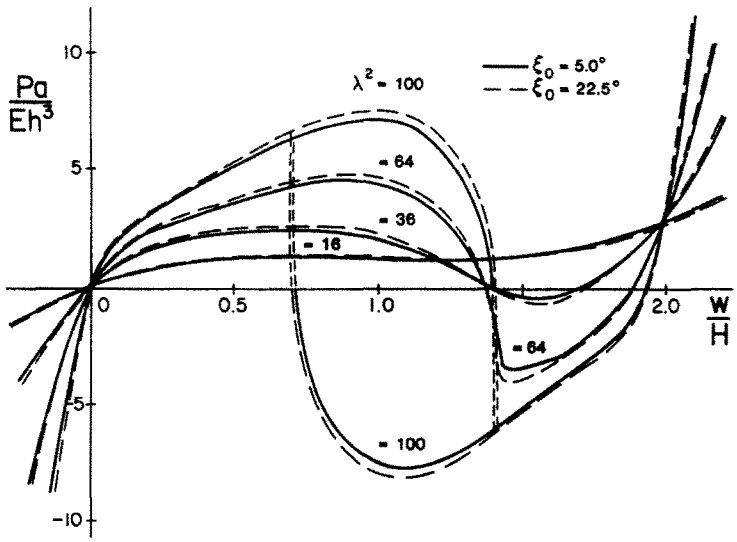

Fig. 4. Load–deflection curves for shallow shells.

eversion, except for a small dimple at the centre. State F has the same apex deflection as E, but it has a significantly different shape and apex loading, and its strain energy is approximately 30% less. From F to G, the reverse load required to maintain a particular deflection decreases. At G, the cap is *everted* and is in equilibrium without external load. Additional downward loading takes the shell from G to H to J.

As the cap is returned to its initial state with apex displacement-governed deformation, it again follows the curve H–G–F, but a new sequence of equilibrium configurations is produced along F–J–K. At K, the cap snaps back to C (snapback) and returns to B along the everting curve C–B.

One can demonstrate experimentally that snapback, like snapthrough, involves *dynamic* phenomena. Indeed, this was observed in our experiments on spherical rubber caps to be described later. After moving through a sequence of equilibrium states such as C–D–E, the cap reaches a state of unstable equilibrium E. It quickly moves away from this unstable state as some of the strain energy of the cap is converted to kinetic energy. As a new equilibrium F is approached, some of the kinetic energy is converted back to cap strain energy, while the rest is dissipated due to small damping effects in the rubber. This new and stable equilibrium state is very rapidly attained.

Since the analysis performed here neglects inertial effects, our numerical scheme is incapable of finding states of motion between equilibrium points such as E and F. Fortunately, our numerical formulation quickly found post-snapping equilibria, such as F, as we moved away from the pre-snapping equilibrium E. The fact that our analysis produced no other equilibrium states for apical loading attests to the dynamic nature of the problem in the snapping domain. Furthermore, it suggests that to find such equilibria, we would need to allow for and find the *distributed loading* necessary to maintain them.

Figures 4 and 5 show the load–deflection curves for shallow and hemispherical shells, respectively. From Fig. 4, it is clear that the results are essentially independent of ξ_0 for $\xi_0 \leqslant 22.5°$. This value corresponds to $H/L = 0.20$, which is slightly beyond the common limit of $H/L = 1/6$ for shallow shells. This is reasonable in view of the fact that the axial coordinate of an undeformed spherical cap measured from its base is

$$z = H - a\left\{\frac{\xi^2}{2!} - \frac{\xi^4}{4!} + \cdots\right\} \tag{38}$$

which simplifies to the approximation

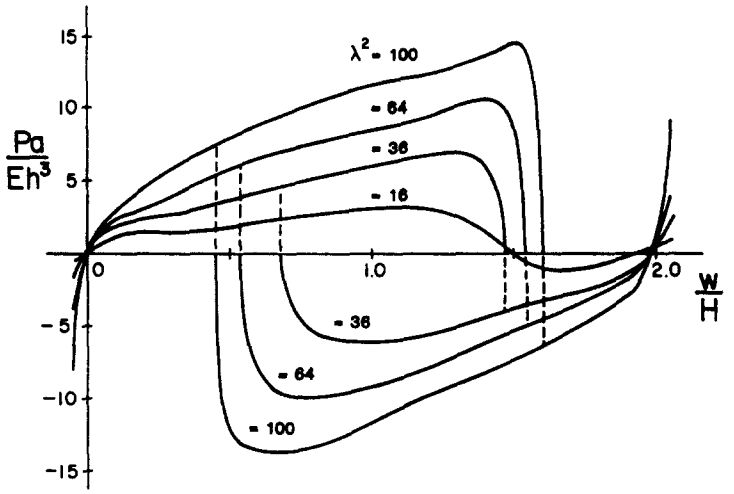

Fig. 5. Load–deflection curves for hemispherical caps.

$$z = H\{1-(R/L)^2\} \tag{39}$$

when the cap is shallow. Equation (39) indicates that all shallow spherical caps have the same essentially parabolic shape and differ from one another only in the shell rise H. In other words, all *shallow* spherical caps can be mapped on to each other by simply scaling their radial and axial coordinates. Such a mapping is *not* possible for non-shallow spherical caps, and explains in part (consider mappings of the standard shallow shell equations) why their response differs from that of shallow caps.

The mechanical response of a spherical cap is due to a combination of *membrane* effects and *bending* effects. The former are characterized by symmetry in load–deflection behaviour between the virgin and everted states. In the absence of any bending effects, a hinged spherical cap would be free to assume a stress-free spherical everted shape. The load–deflection response of the everted cap would be identical to that of the uneverted cap. For thin caps (e.g. $\lambda^2 = 100$), bending stresses are small and their effects are negligible. This is verified in Fig. 3 by the almost perfect symmetry between the load–deflection curve portion A–B–C–D–E of the virgin cap with the portion H–G–F–J–K of the everted cap, as well as by the symmetry between corresponding meridian contours. The only evidence of bending effects is seen near the edge of the cap where they cause slight curvature differences between corresponding meridian contours such as C and F.

As the cap becomes thicker, λ^2 becomes smaller and bending effects which increase as $h^3 \cong (\lambda^2)^{-3}$ increase more quickly than membrane effects which increase as $h \cong (\lambda^2)^{-1}$. Thus, bending effects become relatively more important until they eventually predominate. Bending behaviour is characterized by monotonic load–deflection behaviour. An increasing *asymmetry* is thus seen in Fig. 4 as λ^2 decreases, whence at $\lambda^2 = 16$ the bending effects become so much stronger than *non*monotonic membrane effects that the load–deflection response of the cap becomes monotonic. Similar behaviour occurs in hemispherical caps as shown in Fig. 5, except that here membrane effects are more influential because of the greater depth of the shell.

As is illustrated in Fig. 4, a force-free everted state does not occur in sufficiently thick shells. The self-equilibrating everted state is possible in thinner caps since bending effects are then sufficiently reduced that they can be overcome by membrane forces. Otherwise, the edges of the cap tend to roll back and restore the shell to its rest position. Two important features are observed at the edge of the everted meridian contour (see Fig. 3). To begin with, the meridian edge *curvature* has the same sign here and in every other configuration as it does in the initial state, since membrane effects must operate along a sufficient distance from the edge of the cap before sufficient force is developed to reverse meridian curvature. Secondly, the edge *slope* is of opposite sign here compared to the initial configuration. This is clearly necessary if membrane hoop effects which produce inward radial forces, are to

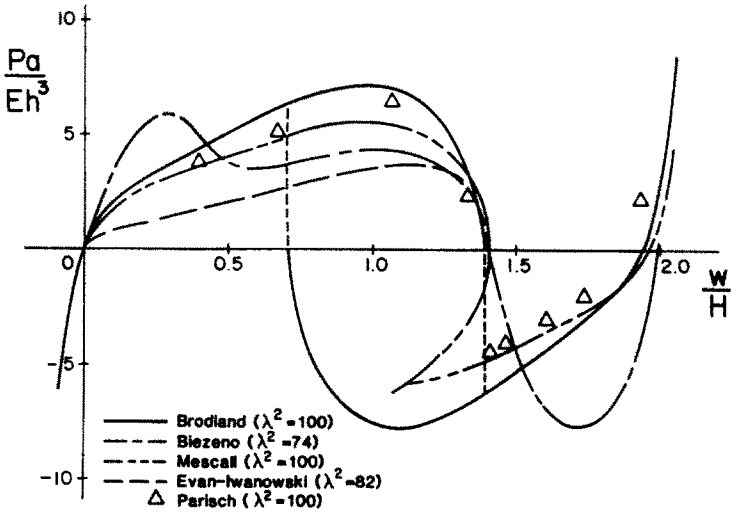

Fig. 6. Comparative load–deflection curves.

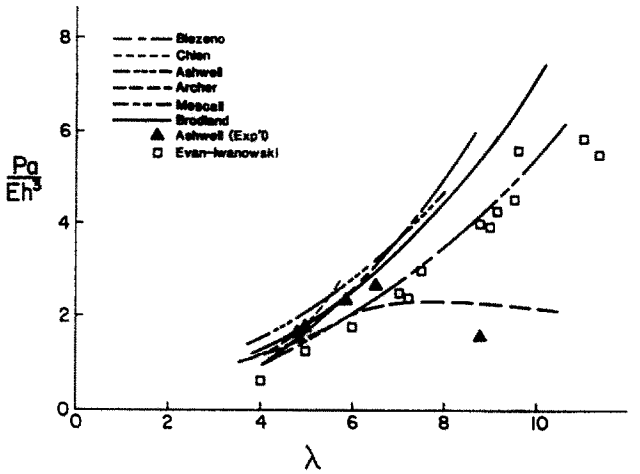

Fig. 7. Critical loads.

prevent bending effects from rolling the edges down and returning the cap to its rest configuration.

Figure 5 shows that the load–deflection curves for hemispherical shells are very similar in shape to those of shallow shells. We point out that the knee in the curve at the critical load is somewhat higher and much sharper for the deep shell case. The meridian contours of a hemispherical shell (not shown) are similar to those of the shallow caps, except that the radial displacements, especially at the edge, are more pronounced.

Figure 6 presents a comparison of the load–deflection curve obtained here for $\lambda^2 = 100$ with those available from the cited literature. The differences are most predominant in the post-buckling region.

For many practical applications, it is the critical load P_c which is of primary interest. Figure 7 shows the critical load P_c as a function of λ. Curves calculated by Biezeno[11], Chien and Hu[12], Ashwell[13], Archer[14], and Mescall[18] are also shown, as are the experimental values obtained by Ashwell[13] and Evan-Iwanowski *et al.*[15]. The critical load calculated here is in good agreement with curves calculated by other researchers. Furthermore, the curve calculated here predicts slightly higher values of P_c than have been obtained experimentally. Theoretical values of P_c must necessarily be higher than those obtained experimentally, as even the small imperfections which are always present in specimens cause the shell to collapse at a lower load.

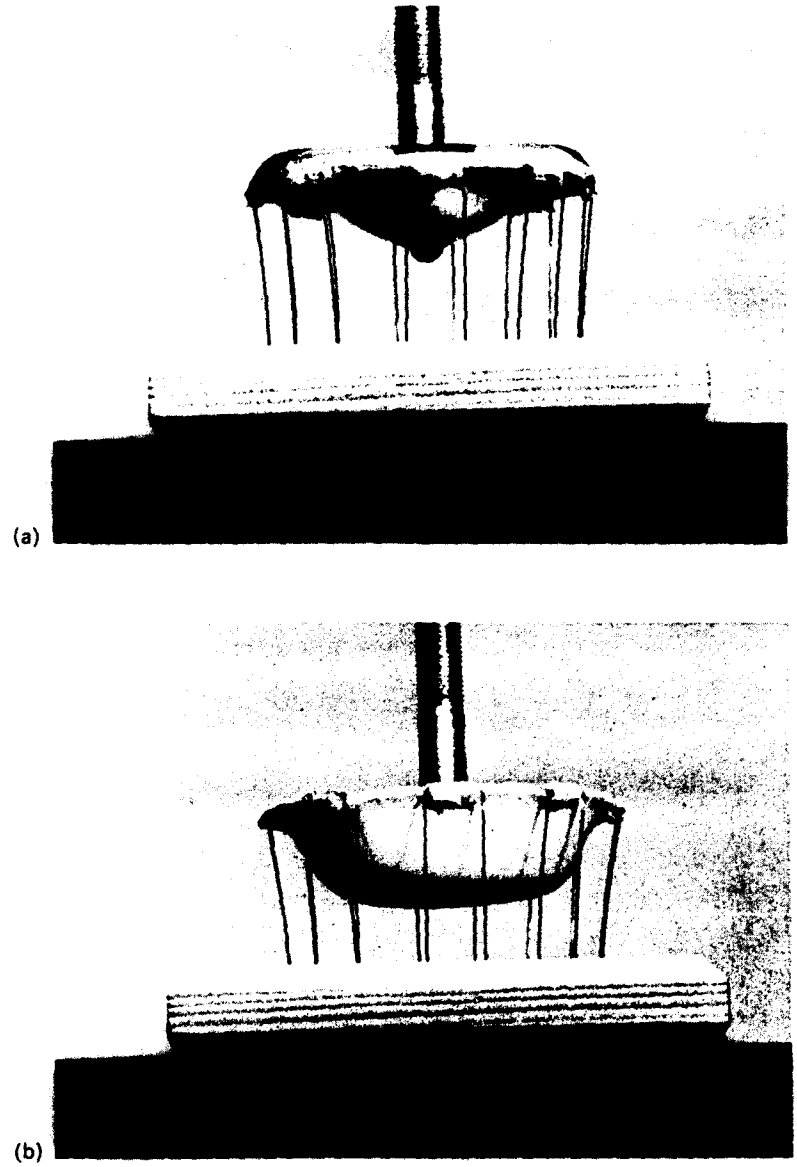

Fig. 10. Photographs of a deformed hemispherical cap: (a) configuration produced on path to eversion; (b) configuration produced on return path.

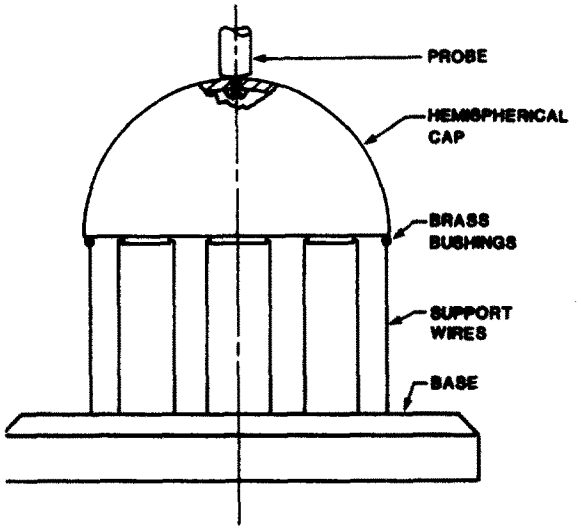

Fig. 8. Experimental apparatus.

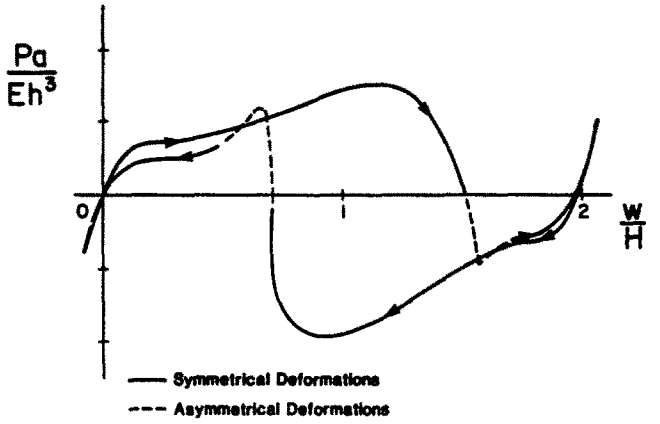

Fig. 9. Experimental load–deflection curve.

Since the load–deflection curves and snapping behaviour obtained herein are significantly different from those published in the literature, a supplementary experimental investigation was performed. The primary experimental difficulty in modelling the caps is to support edges against reversing axial loads while ensuring that radial forces and meridional moments are not present at this edge. This difficulty can be overcome by mounting the edges of the cap on cantilevered wires as shown in Fig. 8, with bushings to prevent moment transfer. A reversible load is applied through a radially restrained plunger, attached to the apex of the shell with a small screw. Since facilities were not available to the authors to fabricate rubber specimens, a nearly hemispherical piece of rubber ball with $\lambda^2 = 95$ was used. The specimen had visible imperfections. The deflection to snapping is symmetrical, but the configurations passed through during snapping are not (Fig. 9). The specimen does not assume a symmetrical configuration immediately after snapping. It is not clear whether this is an inherent property of the geometry, a result of imperfections, or a result of material hysteresis. Clearly, however, the experimental curves exhibit the essential features predicted by the numerical analysis. Figure 10 shows photographs of the specimen for an apex deflection of $w^* \cong 1.5$ on the path to eversion and on the return path. These photographs correspond respectively to the points E and F shown in Fig. 3.

Acknowledgements—Assistance with the experiment, provided by M. King, Faculty of Human Ecology, is gratefully acknowledged, as is the partial financial support of the Natural Sciences and Engineering Research Council of Canada.

REFERENCES

1. P. M. Naghdi, The theory of plates and shells. In *Encyclopedia of Physics* (Edited by S. Flugge), Vol. VIa/2, pp. 425–640. Springer, Berlin (1972).
2. A. Libai and J. G. Simmonds, Nonlinear elastic shell theory. In *Advances in Applied Mechanics*, Vol. 23, pp. 271–371. Academic Press, New York (1983).
3. S. S. Antman, Existence and nonuniqueness of axisymmetric equilibrium states of nonlinearly elastic shells. *Archs Ration. Mech. Analysis* **40**, 329–372 (1971).
4. W. A. Nash, Bibliography on shells and shell-like structures. TMB Report 863, U.S. Navy Dept., David Taylor Model Basin, Washington (1954).
5. W. A. Nash, Bibliography on shells and shell-like structures [1954–1956]. Department of Engineering Mechanics Report, University of Florida, Gainesville (1957).
6. A. Kaplan, Buckling of spherical shells. In *Thin-shell Structures: Theory, Experiment and Design* (Edited by C. Fung and E. E. Sechler), pp. 247–288. Prentice-Hall, Englewood Cliffs, New Jersey (1974).
7. M. Gräff, R. Scheidl, H. Troger and E. Weinmüller, An investigation of complete post-buckling behavior of axisymmetric spherical shells. *Z. Angew. Math. Phys.* **36**, 801–821 (1985).
8. C. G. Lange and G. A. Kriegesmann, The axisymmetric branching behavior of complete spherical shells. *Q. Appl. Math.* **39**, 145–178 (1981).
9. G. V. Ranjan and C. R. Steele, Large deflection of deep spherical shells under concentrated load. *Proc. AIAA/ASME 18th Struc., Struc. Dyn. & Mat. Conf.* (San Diego), pp. 269–278 (1977).
10. L. A. Taber, Large deformation mechanics of the enucleated eyeball. *Trans. Am. Soc. Mech. Engrs, J. Biomech. Engng* **106**, 229–234 (1984).
11. C. B. Biezeno, Uber die Bestimmung der 'Durchschlagkraft' einer schwachgekrümmten, kreisformigen Platte. *Z. Angew. Math. Mech.* **15**, 10–22 (1935).
12. W. Z. Chien and H. C. Hu, On the snapping of a thin spherical cap. 9th Int. Congr. Appl. Mech., University of Brussels, p. 6 (1957).
13. D. G. Ashwell, On the large deflection of a spherical shell with an inward point load. *Proc. IUTAM Symp. Theory of Thin Elastic Shells*, Delft, The Netherlands, pp. 43–63 (1959).
14. R. R. Archer, On the numerical solution of the nonlinear equations for shells of revolution. *J. Math. Phys.* **41**, 165–178 (1962).
15. R. M. Evan-Iwanowski, H. S. Cheng and T. C. Loo, Experimental investigations of deformations and stability of spherical shells subjected to concentrated load at the apex. *Proc. Fourth U.S. Nat. Congr. Appl. Mech.*, Berkeley, California, pp. 563–575 (1962).
16. T. C. Loo and R. M. Evan-Iwanowski, Experiments on stability on spherical caps. *Proc. ASCE* **EM3**, 255–270 (1964).
17. P. Wilson and E. E. Spier, Numerical analysis of large axisymmetric deformations of thin spherical shells. *Proc. First AIAA Annual Meeting*, pp. 1716–1725 (1964).
18. J. Mescall, Large deflections of spherical shells under concentrated loads. *J. Appl. Mech.* **32**, 936–938 (1965).
19. J. Mescall, Numerical solutions of nonlinear equations for shells of revolution. *AIAA J.* **4**, 2041–2043 (1966).
20. D. Bushnell, Bifurcation phenomena in spherical shells under concentrated and ring loads. *AIAA J.* **5**(11), 2034–2040 (1967).
21. H. Parisch, Geometrically nonlinear analysis of shells. *Comput. Meth. Appl. Mech. Engng* **14**, 159–178 (1978).
22. H. Cohen and F. Pastrone, Axisymmetric equilibrium states of nonlinear elastic cylindrical shells. *Int. J. Non-Linear Mech.*, **21**, 37–50 (1986).
23. G. W. Brodland, Large axisymmetric deformation of thin shells of revolution. Ph.D. Thesis, Department of Civil Engineering, University of Manitoba, Winnipeg, Manitoba (1985).
24. A. Libai and J. G. Simmonds, Large-strain constitutive laws for the cylindrical deformation of shells. *Int. J. Non-Linear Mech.* **16**, 91–103 (1981).
25. J. G. Simmonds, The strain energy density of rubber-like shells of revolution undergoing torsionless, axisymmetric deformation (axishells). Appl. Math. Rep. No. 85-01, University of Virginia (1985).
26. L. A. Taber, On approximate large strain relations for a shell of revolution. *Int. J. Non-Linear Mech.* **20**, 27–39 (1985).